ACS OMEGA

http://pubs.acs.org/journal/acsodf

Article

# Biomass Hierarchical Porous Carbonized Typha angustifolia Prepared by Green Pore-Making Technology for Energy Storage

Shuya Wang, Yidong Mei, Zishuo Shao, Jingru Wang, Zhenzhen Tan, Zurui Qiu, Minghao Wang, and Hong Zheng*

Cite This: *ACS Omega* 2023, 8, 1353−1361

Read Online

ACCESS | Metrics & More | Article Recommendations | Supporting Information

**ABSTRACT:** The cost-effective biomass-derived carbon with high electrochemical performance is highly desirable for the sustainable development of advanced energy storage devices. In this manuscript, *Typha angustifolia* with a large output and loose porous characteristics was selected as the raw material of biomass. In the synthesis process, $KHCO_3$, which is more environmentally friendly, is used as a pore-forming agent, and the low-cost, easy-to-clean fluxing agent NaCl is used to assist the pore-forming process. Based on the analysis of thermogravimetric-infrared test results, the calcination procedure of porous carbon was designed reasonably, so that the functions of the pore-forming agent and fluxing agent could be fully exerted. Its high electrochemical performance is attributed to combined contributions from high surface area and hierarchical porous structures. The as-prepared carbon also showed an outstanding capacitance of 317.2 F/g at a current density of 1 A $g^{-1}$ and a high capacitance retention of over 97.83% after 5000 cycles at a current density of 4 A $g^{-1}$. This work provides an outstanding renewable candidate and a feasible route design strategy for the fabrication of high-performance electrodes.

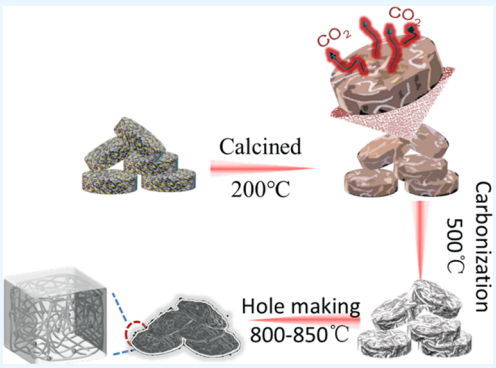


## 1. INTRODUCTION

With the continuous depletion of energy sources and environmental deterioration, people have put forward higher requirements for cleaner production and green low-carbon development. The international problem that needs to be solved to realize a low-carbon society is to reduce the use of carbon-based underground resources and to strongly encourage the use of carbon-neutral biomass resources.[1] The development needs of a low-carbon society force people to develop renewable clean energy and supporting energy storage and conversion devices. New electrochemical energy storage devices have emerged as the times require and are indispensable in modern society.[2] Among them, supercapacitors, one class of electrochemical energy storage devices, have gradually become a research hotspot and play an important role in efficient exploitation of clean and renewable energy sources, due to their rapid charge/discharge speed and long cycle life.[3]

The electrode material is the key to the performance of supercapacitors.[4] The foremost way to enhance the energy density of supercapacitors is to use appropriate high-performance electrode materials.[5] Therefore, some researchers are constantly trying to find excellent electrode materials to improve the energy density of supercapacitors while maintaining their long cycle life. Among them, carbon materials, as one of the electrode materials, have been widely concerned and applied. Carbon materials have an extensive range of environmental applications such as anaerobic digestion,[6] supercapacitors,[7] and solar cells,[8] benefiting from their appreciable surface area, variable pore structures, and a variety of sources.[9] However, common powdered carbon presents problems involving environmental pollution and inconvenient utilization.[10] In fact, all the carbon-based materials and their various structural forms including activated carbon, CNTs, graphene, and carbon aerogels were used as an active electrode material for electrochemical double-layer capacitors.[11] Among all these carbon-based materials, biomass porous carbon based on bio/organic waste is a very popular raw material used in high-level applications due to its advantages of high porosity, high electrical conductivity, suitable pore structure, and good stability.[12] Carbon materials with hierarchically porous structures have attracted increasing attention in recent years, especially for use as electrodes in electrochemical energy storage devices.[13] Numerous researchers have focused on the selection of biomass materials and the development of strategies to fabricate hierarchical porous materials.

**Received:** October 20, 2022
**Accepted:** December 13, 2022
**Published:** December 23, 2022

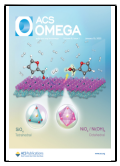





https://doi.org/10.1021/acsomega.2c06782
*ACS Omega* 2023, 8, 1353−1361

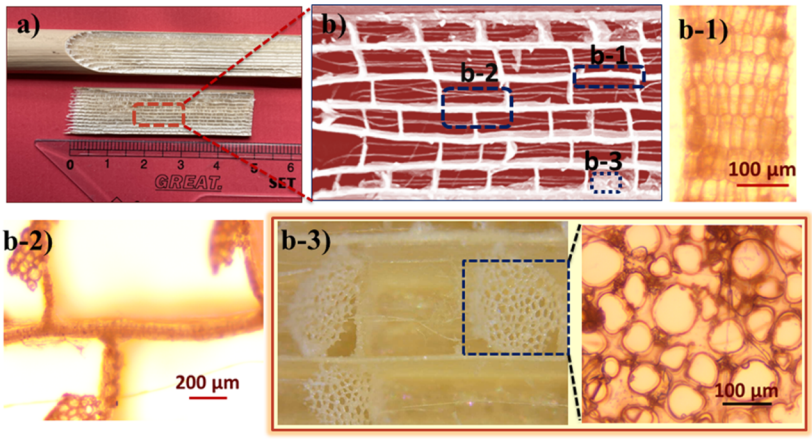


**Figure 1.** a) Unenlarged real image and (b) magnified image of the part selected by the dotted box in Figure 1a taken with a normal camera; (b-1, b-2 and b-3) optical microscope-magnified view of different parts selected by the dotted box in Figure 1b.

*Typha angustifolia* can effectively absorb nitrogen, phosphorus, and other elements in the water body and has the hierarchical porous structure for transporting ions, water, and oxygen during the metabolic process.[14] If a large number of plant residues are not harvested or removed in time, they will cause water pollution and deterioration of water quality. The timely harvest and resource utilization of Typha angustifolia are the key to the scientific management. In this study, Typha angustifolia was used as the bio-active material to prepare porous carbon for supercapacitor electrode materials.

For most carbon materials, activation is mainly to increase the specific surface area of the material by creating a large number of pores. The activation steps are critical to the formation of porosity and different functional groups in the carbon electrode materials of electric double layer capacitance (EDLC) and pseudocapacitance.[15] Compared with the commonly used KOH activator, $KHCO_3$ is less corrosive, has no special requirements for the calcination equipment, and is easier to wash and more environmentally friendly after calcination. Moreover, the decomposition of $KHCO_3$ produces more gas and creates a good expansion effect, which is beneficial to pore formation and production of hierarchically porous carbons.[16]

The research idea we choose in this manuscript is to prepare porous carbon with a hierarchical pore structure using Typha angustifolia as a biomass active raw material. During the synthesis, $KHCO_3$, which is more environmentally friendly and easier to clean after calcination, was used as a pore former to generate a porous structure. The use of NaCl as a template at low temperature and a suitable reaction medium at high temperature provide another pathway for porous formation. This work paves the way for the ready conversion of abundant biomass into high-value engineering products for energy-related applications.

## 2. EXPERIMENTAL SECTION

**2.1. Material Syntheses.** Biomass porous carbon was synthesized by the calcination method after solid-phase mixing in which the pore-forming agent ($KHCO_3$) and fluxing agent (NaCl) were introduced at the same time. The raw materials are listed as follows: $KHCO_3$ (99%, Aladdin) and NaCl (99%, Aladdin). The synthetic steps are shown below. The biomass material is washed, dried, and then pulverized to fine powder. The biomass material, pore-forming agent ($KHCO_3$), and fluxing agent (NaCl) were mixed according to a mass ratio of 1:3:6 and placed in an agate mortar for pre-grinding for 10 min. The pre-milled mixture was added to the ball mill, and a certain program was set for ball milling. Part of the ball-milled mixture is pressed into tablets, and the other part is not pressed. The tableted and non-tableted samples were calcined by a certain temperature program to obtain porous carbons, which were named PC-Tablet and PC-Non-tablet, respectively. The solid product was washed several times with distilled water, collected, and dried at 60° C for use.

**2.2. Material Characterization.** The thermogravimetric-infrared spectrometry (TG-IR, PE TGA4000 + SP2) instrument is used to test the sample weight loss and gas production in a certain temperature range, which can assist in determining the calcination temperature program and reaction mechanism. The characterization of the crystal structure was carried out mainly on a Bruker D8 Advance X-ray diffractometer with a diffraction angle of 5−90. Thermo Scientific K-Alpha X-ray photoelectron spectroscopy (XPS) using Al K$\alpha$ rays as the excitation source was used to further aid in the specification of the structural information of the sample. The morphological characteristics of bio-charcoal were mainly outlined by scanning electron microscopy (SEM, FEI Scios 2 HiVac), field emission transmission electron microscopy (TEM, FEI Talos F200s), and an auxiliary mapping test. The $Na^+$ content in the cleaning solution was determined by inductively coupled plasma optical emission spectrometry (ICP-OES, Thermo Scientific iCAP 6500 Duo). The surface wettability of porous carbon materials is completed using a contact angle/surface tension measuring instrument (Germany Dataphysics OCA20).

**2.3. Electrochemical Characterization.** Porous carbon, carbon black (conductive agent), and polytetrafluoroethylene (binder, PTFE) were weighed in a mass ratio of 8:1:1. The active material and carbon black are ground to make the two evenly mixed before use. The PTFE emulsion was diluted with alcohol to a concentration of 10% and then added dropwise to the mixture of the ground-active material and carbon black according to the mass ratio. Then, an appropriate amount of absolute ethanol was added and dispersed by ultrasonication until it became viscous. The viscous mixture was applied evenly to half the area on one side of the pretreated nickel foam (dimensions: 1 cm × 2 cm). The coated nickel foam was put into a drying oven and vacuum-dried at 60 °C for 10 h, and


https://doi.org/10.1021/acsomega.2c06782
ACS Omega 2023, 8, 1353−1361

then, the working electrode for testing was obtained by applying a certain pressure in the tableting machine.

Galvanostatic charge−discharge (GCD), CV cycling, and electrochemical impedance spectroscopy performance tests were carried out using the assembled three-electrode system. The nickel foam coated with the mixed electrode material described above was used as the working electrode. A platinum electrode counter electrode, Hg/HgO reference electrode, and the porous carbon as working electrodes were used to perform the electrochemical measurements in a 6 mol $L^{-1}$ KOH electrolyte solution. The electrochemical tests were all carried out on the electrochemical workstation. A three-electrode system was used to test its electrochemical impedance spectroscopy with a frequency range of $10^{5}$−$10^{-2}$ Hz.

The specific capacitance ($C$, F $g^{-1}$) of the supercapacitor in the three-electrode system was calculated on the GCD curves according to the following equation[17]

$$C = \frac{I\Delta t}{m\Delta V} \quad (1)$$

For the abovementioned equations, $I$, $m$, $\Delta t$, and $\Delta V$ are the discharge current (A), effective weight of the material (g), discharge time (s), and effective voltage excluding voltage drop (IR drop) in the discharge process (V), respectively.

## 3. RESULTS AND DISCUSSION

### 3.1. Structural and Morphological Characterization.

The image shown in Figure 1 can clearly reflect the original appearance of Typha angustifolia. In order to show its original structure before calcination more clearly, the part selected by the dotted box in Figure 1a was gradually enlarged by ordinary camera and optical microscope, and the grid structure is shown in Figure 1b. The different sides of the grid structure are magnified again by the optical microscope, as shown in b-1, b-2, and b-3 of Figure 1. The structures of different sides are slightly different, but they can all show the natural advantages of Typha angustifolia morphology. As an aquatic plant, Typha angustifolia has a natural pore structure that facilitates the transport of water and nutrients, and these pores are interwoven to form a spider web-like structure. The above-mentioned structures provide natural advantages for the smooth progress of the subsequent pore-making process.

Different types of pores play different roles in the electrochemical performance of carbon materials. Micropores are the primary sites for charge storage and are essential for high energy storage; mesopores can accelerate ion diffusion in electrodes and improve power performance at high current densities; macropores act as ion buffer storage, providing short diffusion distance and facilitating rapid transport of electrolyte ions.[18] Figure 2 shows a schematic diagram of the pore-making process chosen herein. Hierarchically porous carbons with a high surface area have been synthesized by a salt template-assisted chemical activation approach using biomass Typha angustifolia as a carbon precursor. An important characteristic of our synthesis strategy is that the carbonaceous matter is immersed in a melted mixture constituted by the activating agent and NaCl. *Typha angustifolia* is pyrolyzed in the presence of NaCl, serving as a template and reaction medium, and $KHCO_3$, acting as both a template and activating agent. The detailed synthesis process is as follows: $KHCO_3$, NaCl, and biomass materials are mixed by solid-phase grinding and pressed under a pressure of 2 MPa. The pressed samples are calcined by a certain heating program, and the calcination will

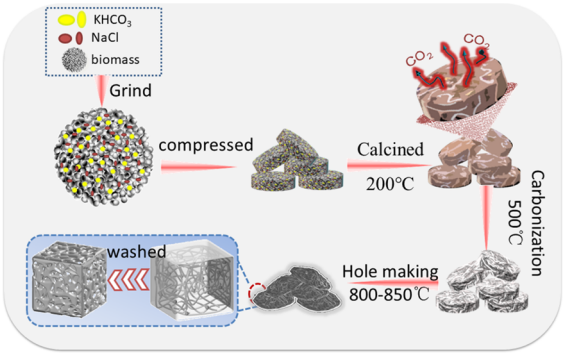


**Figure 2.** Diagram of the formation process of porous carbon with the gradient pore structure.

go through the processes of pore expansion (the releasing of carbon dioxide by calcining $KHCO_3$), carbonization, and secondary pore making by melting.[19] In order to more intuitively illustrate the necessity of the tableting process after the samples are mixed, the subsequent morphology and performance tests in this paper compare the two methods of being compressed and uncompressed.

The choice of the heating program (heating rate, holding temperature, and holding time) during calcination will have a great influence on the morphology of the product. In order to facilitate the determination of a more reasonable heating program, TG-DTG and TG-IR tests were first performed, and the results are shown in Figure 3a,b. From the analysis of TG-DTG test results, the heating process is roughly divided into three stages. The first stage is before 300 °C, and there is a large variation at around 200 °C. The second stage is between 300 and 700 °C, with a smaller amplitude at around 500 °C. The third stage is above 700 °C, and there is another large variation at around 850 °C. Combined with the TG-IR data, it can be speculated that 200 °C corresponds to the decomposition temperature of potassium bicarbonate (eq 1), 500 °C corresponds to the carbonization reaction, and 850 °C corresponds to the pore-forming reaction temperature (eqs 2 and 3). In order to better control the degree of reaction in different reaction stages, a temperature program with three stages (200, 500, and 800 °C) was set as shown in Figure 3c.

$$2KHCO_3 \rightarrow K_2CO_3 + CO_2 + H_2O \quad (2)$$

$$K_2CO_3 + 2C \rightarrow 2K + 3CO \quad (3)$$

$$K_2CO_3 \rightarrow K_2O + CO_2 \quad (4)$$

The selection of molten salt is also based on the test results of TG-DTG and TG-IR. The choice of different melts has a great influence on the morphology of the product.[20] A porous carbon matrix is created depending on the type and amount of activating agent, reaction time, and the temperature.[21] In order to make the addition of the fluxing agent play a better role, it is necessary to make the melting temperature of the selected fluxing agent slightly lower than the pore-making temperature. The molten salt must be stable, readily available, inexpensive, and easily washed away with water. After sufficient comparison and selection, this paper chooses molten salt NaCl as the fluxing agent. The melting points of NaCl and KCl are 800 °C and 774 °C, respectively.[19] On the one hand, compared with KCl, the melting temperature of NaCl molten salt is lower than the pore-forming temperature and closer to the pore-forming temperature. On the other hand, NaCl is low cost and easy to


https://doi.org/10.1021/acsomega.2c06782
ACS Omega 2023, 8, 1353−1361

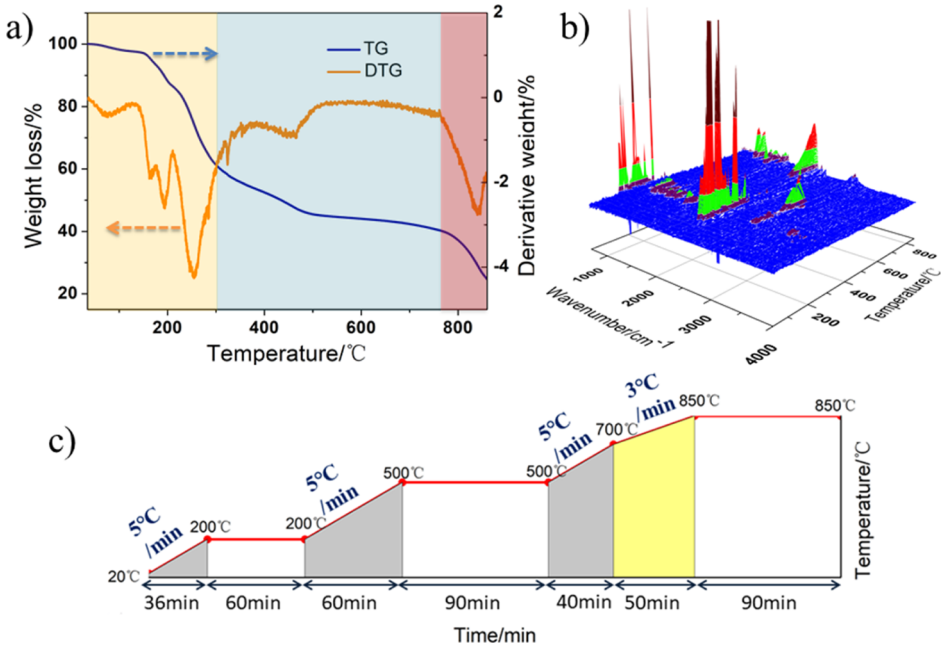


**Figure 3.** Image related to selection of calcination temperature. (a)TG-DTG curve; (b) 3D curve of TG-IR; and (c) temperature program of the vacuum calcination process.

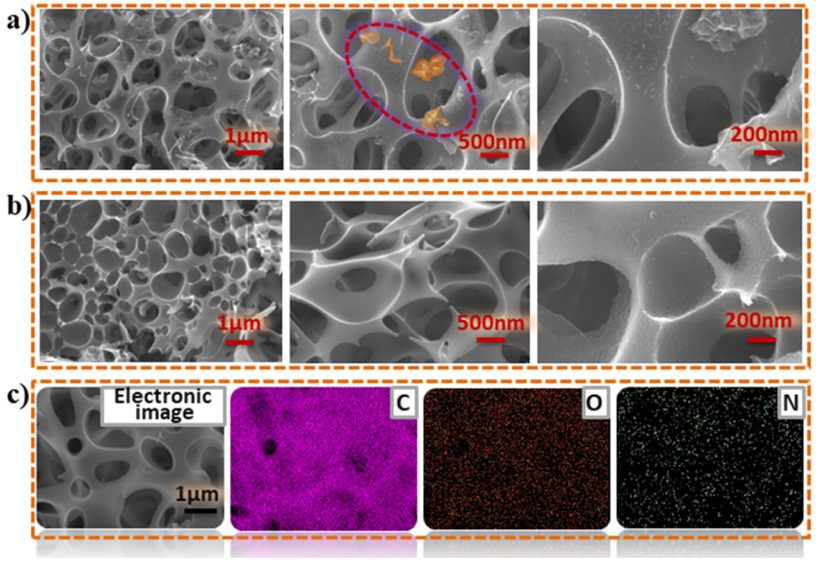


**Figure 4.** SEM images of porous carbons obtained after calcination in two ways: (a) PC-Non-tablet, (b) PC-Tablet, and (c) mapping of PC-Tablet.

clean and is more suitable for molten salt used in the pore-making process. This technique is beneficial to create a sufficient pore structure along with high specific surface area and good conductivity, which are the primary criteria to select any electrode for supercapacitors.

The successful formation of the porous carbon sample is confirmed by performing various structural characterization techniques. SEM and TEM tests were used to confirm the morphology of the samples. Figure 4 shows that samples prepared by both methods appear to be porous at different magnifications. The creation of the porous network can be attributed to the multi-step release of gas attributable to $KHCO_3$ and the action of the fluxing agent. $KHCO_3$ activation introduces pores into the framework by chemically reacting with carbon to form a porous foam-like interconnected carbon framework. The first step is the decomposition of $KHCO_3$ to release $K_2CO_3$ and $CO_2$, and then, $K_2CO_3$ can further react to release CO and $CO_2$ gas, thereby forming more pores on the carbon matrix.[21b] These potassium compounds can be embedded in the carbon matrix in the form of $K_2O$, and these potassium compounds can be easily removed by washing.[22] The addition of the fluxing agent NaCl achieves good mixing of the pore-forming agent with the biomass material. When approaching the temperature at which the pore-forming reaction occurs, the fluxing agent appears in a molten state and becomes a medium for the combination of the pore-forming agent and the biomass. The formation of the contact medium in the molten state can increase the effective utilization of the pore former.

The pores of PC-Non-tablet (Figure 4a) have a certain degree of inhomogeneity compared to those of PC-Tablet (Figure 4b). The PC-Tablet has better porosity because of the



https://doi.org/10.1021/acsomega.2c06782
ACS Omega 2023, 8, 1353−1361

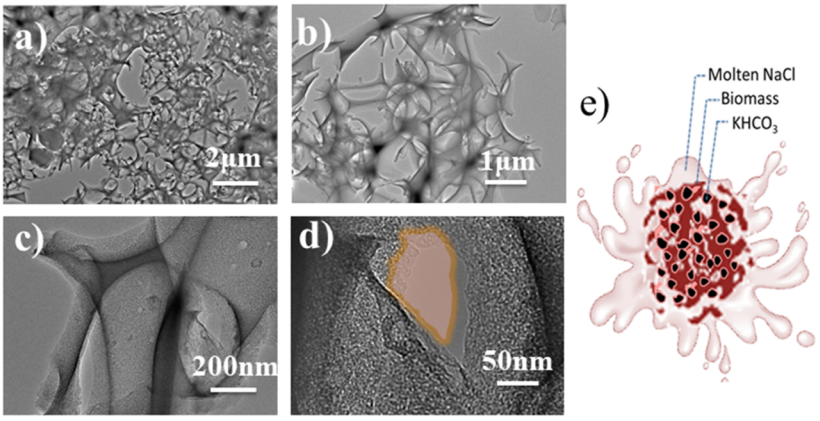


**Figure 5.** TEM images of porous carbons obtained after calcination of PC-Tablet. (a–d) TEM with different magnifications. (e) Contact state of the pore-forming agent, molten NaCl, and biomass material under tableting conditions.

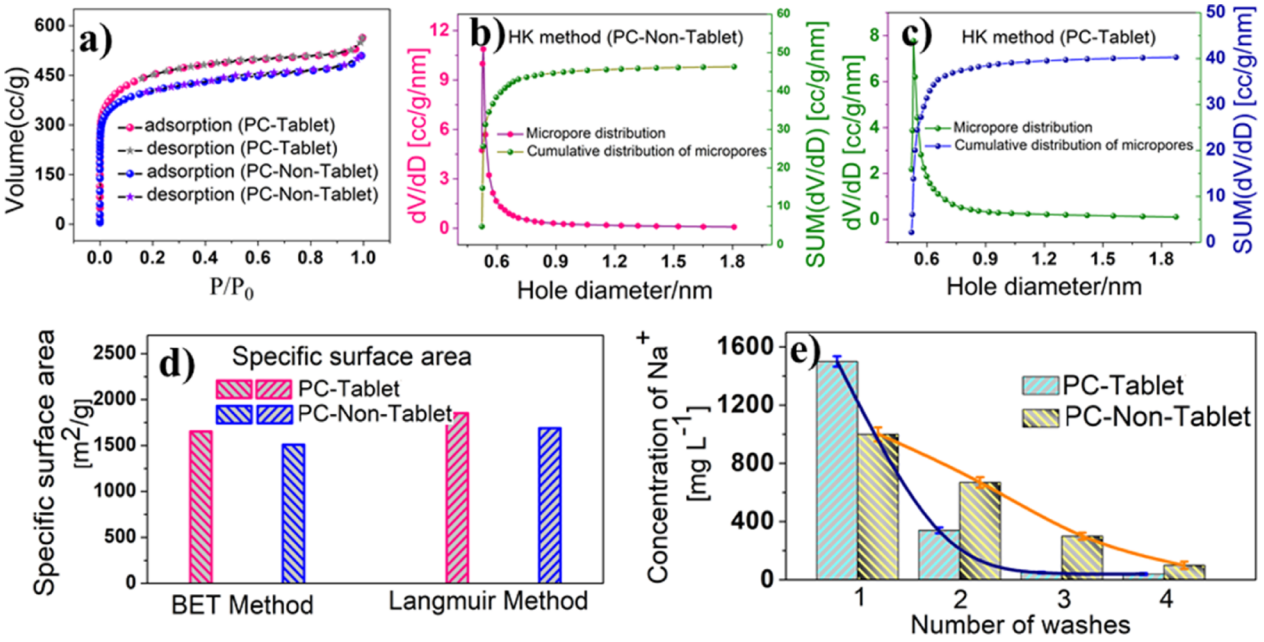


**Figure 6.** Experimental results of $N_2$ adsorption and the cleaning effect of pore-forming agents. (a) Adsorption and desorption curves of BET test, (b,c) pore volume distribution curves of HK methods for PC-Non-tablet and PC-Tablet samples, (d) comparison of specific surfaces, and (e) $Na^+$ concentration in the aqueous washing solution of calcined porous carbon precursors.

close and uniform contact of the pore-forming agent, and the fluxing agent and the biomass material can be achieved during the calcination process. Uniform and ordered macropores in dimensions larger than 300 nm and through-holes composed of interconnected walls were observed. The macropores provide sufficient spaces to buffer the ions so that they can get easy access to the inner surface of the active materials.[23] Figure 4c shows a mapping image of the C, O, and N elements of the PC-Tablet material, and the O and N elements achieve a uniform distribution in the porous carbon material. The inherent heteroatom calcination process can form functional groups, such as carboxyl, which makes the better contact between the fluxing agent and the biomass carbon matrix during the melting process, and is conducive to the smooth porous formations. Therefore, these inherent heteroatoms are beneficial to improve the porosity of porous carbon materials.[24] The hierarchical pore structure combining macro-, meso-, and micropores takes advantages of the synergistic effect between pores at different length scales, which are in favor of improving the electrochemical performances of the active materials compared with pores with a single length scale.[25] The TEM images of the PC-Tablet material can reflect its porous structural information more clearly (Figure 5a–d). At low temperatures, NaCl acts as a template, generating large voids in the carbonaceous matter, while at higher temperatures, it provides a confined reaction medium as a consequence of the formation of a melted phase. The contact state of the pore-forming agent, molten NaCl, and biomass material under tableting conditions is shown in Figure 5e. The interconnected pores can provide fast channels for ion/charge or substance transport.[26]

Another proof of the presence of heteroatoms in porous carbon is obtained from the XPS analysis results in Figure S1. Figure S2 shows the XRD spectra of PC-Non-tablet and PC-Tablet samples in which the observed peak positions are well-matched with the previous literature.[27] The sample shows peaks in the $2\theta$ range of 23–27° (002) and 41–43° (100) that correspond to the presence of turbostratic carbon with low


https://doi.org/10.1021/acsomega.2c06782
ACS Omega 2023, 8, 1353–1361

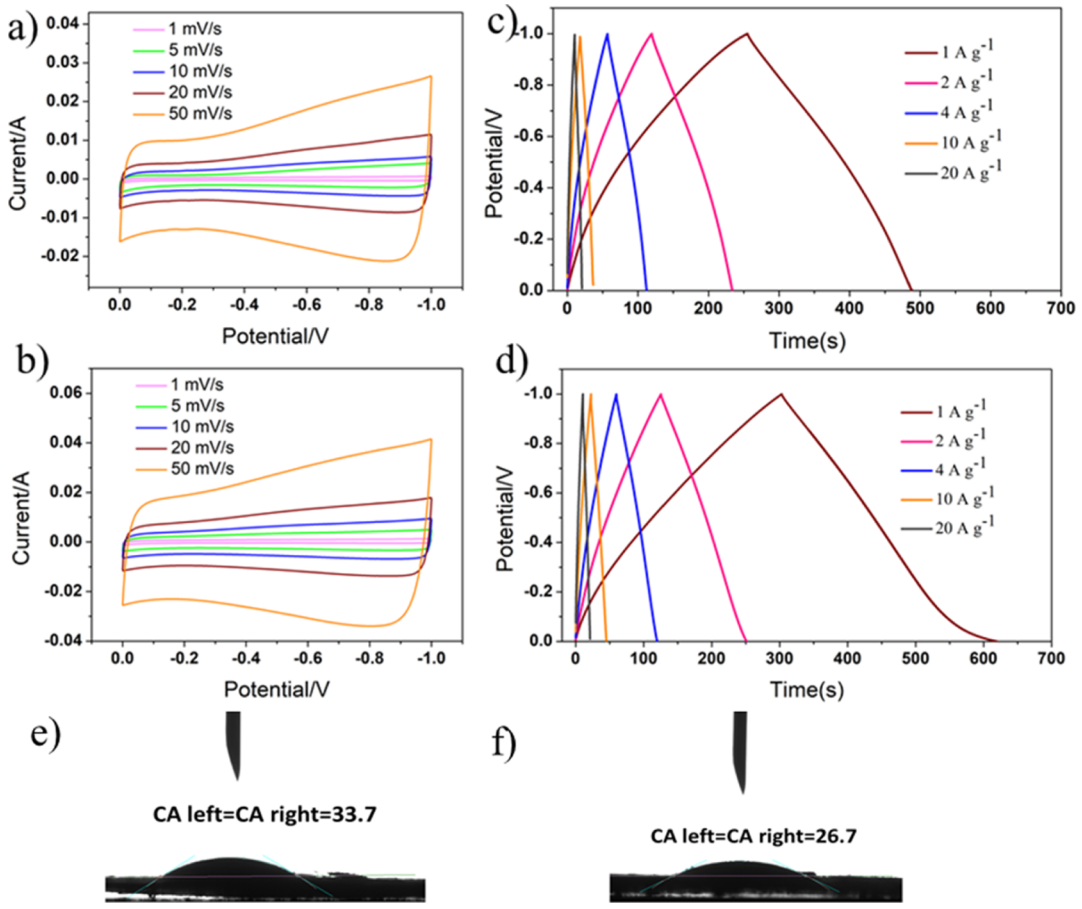


**Figure 7.** CV curves of PC-Non-tablet and PC-Tablet with the scan rates ranging from 1 to 50 mV $s^{-1}$[(a) PC-Non-tablet and (b) PC-Tablet]; GCD curves of PC-Non-tablet and PC-Tablet with the specific currents ranging from 1 to 20 A $g^{-1}$[(c) PC-Non-tablet and (d) PC-Tablet]; and static contact angle graphical results [(e) PC-Non-tablet and (f) PC-Tablet].

crystallinity.[28] In addition, the increase in intensity at the low-angle scattering peak corresponds to a high density of micropores.[24]

The porous structure of the hierarchically porous carbons was analyzed by means of $N_2$ physisorption experiments at −196 °C. The $N_2$ adsorption isotherms of the carbons prepared under different experimental conditions are shown in Figure 6. All of the isotherms display a sharp increase in the amount of nitrogen adsorbed at very low relative pressures, indicative of a porosity made up mainly of micropores (Figure 6a). The linear correlation line for the BET test is shown in Figure S3. Figure 6b,c shows the pore distribution curve and cumulative pore distribution curve of the HK method. The existence of large quantities of micropores enhances the electric-double-layer capacitance of the active materials.[29] The presence of large mesopores or macropores is also evidenced by the pronounced nitrogen uptake at high relative pressures ($p/p_0 > 0.9$). The existence of mesopores can be confirmed by the BJH adsorption distribution curve, as shown in Figure S4. The "multiple synergistic" effect of the abovementioned features is beneficial to improve the electrochemical energy storage performance of the material. Figure 6d shows that the PC-Tablet porous carbon exhibits a higher specific surface area, thereby providing more active sites for electrochemical reactions.

In this experiment, the calcined product obtained is a mixture of porous carbon and soluble salts such as sodium chloride, which needs to be washed with distilled water before use. Water, as a scarce resource in China at this stage, needs to be highly concerned about its usage. In order to compare the influence of tableting or not on the cleaning effect, this part conducts sampling tests on the cleaning process of the porous material obtained by calcination in two ways. The specific operation steps are as follows: the calcined sample is subjected to four ultrasonic washing and suction filtration processes, and the sodium ion content in the aqueous solution after each suction filtration is tested. The result obtained is shown in Figure 6e. Since the electrode material obtained by calcination after tableting contains relatively high concentrations of sodium chloride and unreacted potassium bicarbonate in the washing solution of the first cleaning stage, recycling can be considered.

### 3.2. Electrochemical Performance Characterization.

Figure 7a,b presents the CV plots of the EDLC collected by a three-electrode system, at different scan rates ranging from 1 to 50 mV $s^{-1}$ within a voltage of −1 to 0 V. The CV curves of the PC-Non-tablet and PC-Tablet electrodes taken at varying scan rates featured a rectangular shape which is an ideal EDLC behavior during the potential window of −1 to 0 V. Figure 7c,d shows the GCD plots for PC-Non-tablet and PC-Tablet electrode materials at potentials ranging from −1 to 0 V. The area covered by the CV curve of the three-electrode system with PC-Tablet as the active material is significantly larger than that of PC-Non-tablet, which indicates that the PC-Tablet carbon material has a larger specific capacitance (Figure S5). The GCD plots at varying specific currents displayed a



https://doi.org/10.1021/acsomega.2c06782
ACS Omega 2023, 8, 1353−1361

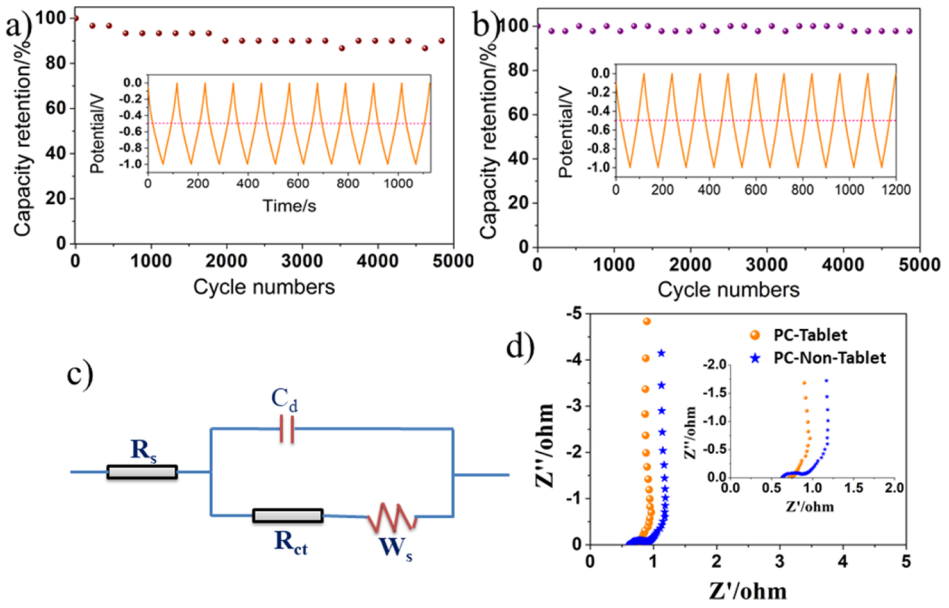


**Figure 8.** Cycling stability at a current density of 4 A/g under a certain cycle of PC-Non-tablet (a) and PC-Tablet (b); (c) equivalent-circuit diagram; and (d) Nyquist plots with an enlargement of the high-frequency region as the inset of PC-Tablet and PC-Non-tablet.

triangular shape, therefore confirming the capacitive behavior. For the same specific currents, the PC-Tablet electrode material exhibited higher specific capacitance values than the PC-Non-tablet. At a current density of 1 A $g^{-1}$, the capacitance of PC-Tablet porous carbon is 317.2 F $g^{-1}$. When the current density increases to 20 A $g^{-1}$, the capacitance of PC-Tablet porous carbon can still be maintained at 212.0 F $g^{-1}$. The comparative data with the research work of relevant biomass carbon materials are shown in Table S1. The better charge storage capacity of PC-Tablet electrode materials can be attributed to the structural characteristics of high specific surface area and pore volume of the porous carbon network. The better wettability of the electrode material can increase the contact between the electrode material and water electrolyte and improve the electrochemical performance of the electrode.[30] Figure 7e,f shows the wettability results of porous carbon electrodes. Compared with PC-Non-tablet electrodes, PC-Tablet possesses dramatically better wettability. The long cycle stability test results in Figure 8a,b also verify the advantages of the PC-Tablet electrode.

The capacitive interface behavior of the electrode materials was further investigated using electrochemical impedance spectroscopy (EIS). The fitted circuit diagram and Nyquist plot of the impedance are shown in Figure 8c,d, respectively. The Nyquist plot has two distinct parts, the high-frequency region is semicircular and the low-frequency region is linear. In the high-frequency region, the solution resistance and charge transfer resistance can be obtained from the intercept on the real axis and the semicircle intercept in the Nyquist plot, respectively. According to this fitting result, PC-Tablet exhibited lower high-frequency resistance, indicating a good contact between the electrolyte and its active material. This phenomenon is mainly attributed to the more uniform porous morphology and higher specific surface area of the as-prepared PC-Tablet porous carbon materials due to the closer contact between the fluxing agent and the biochar precursor during calcination.

## 4. CONCLUSIONS

In summary, a novel carbon material was fabricated by calcining *Typha angustifolia* with synchronous $KHCO_3$ activation and NaCl-assisted melting. The prepared PC-Tablet porous carbon material with Typha angustifolia as a raw material has a unique hierarchical porous structure and showed a large specific surface area (1654 $m^2/g$). As the active material of the supercapacitor, it has excellent electrochemical cycle stability, which is mainly reflected in a retention rate of 97.83% after 5000 cycles in the three-electrode system in the 6 M potassium hydroxide electrolyte. In addition, the environmental friendliness brought by the pore forming agent and fluxing agent is also an advantage to be proposed. Generally, this strategy is an economical and environmentally friendly method for sustainable waste wood management, allowing practical industrial application in electrochemical energy storage systems.

## ■ ASSOCIATED CONTENT

### Supporting Information

The Supporting Information is available free of charge at https://pubs.acs.org/doi/10.1021/acsomega.2c06782.

XPS spectrum, XRD spectrum, linear fitting results, distribution of pore volume with pore diameter of the BJH curve, CV curves, and performance comparison of supercapacitors (PDF)

## ■ AUTHOR INFORMATION

### Corresponding Author

**Hong Zheng** − *College of Environmental Engineering, Xuzhou University of Technology, Xuzhou 221018, China;* orcid.org/0000-0002-4128-5829; Email: zhenghong067@163.com

### Authors

**Shuya Wang** − *College of Environmental Engineering, Xuzhou University of Technology, Xuzhou 221018, China*



https://doi.org/10.1021/acsomega.2c06782
*ACS Omega* 2023, 8, 1353−1361

**Yidong Mei** − *College of Environmental Engineering, Xuzhou University of Technology, Xuzhou 221018, China*
**Zishuo Shao** − *College of Environmental Engineering, Xuzhou University of Technology, Xuzhou 221018, China*
**Jingru Wang** − *College of Environmental Engineering, Xuzhou University of Technology, Xuzhou 221018, China*
**Zhenzhen Tan** − *College of Environmental Engineering, Xuzhou University of Technology, Xuzhou 221018, China*
**Zurui Qiu** − *College of Environmental Engineering, Xuzhou University of Technology, Xuzhou 221018, China*
**Minghao Wang** − *College of Environmental Engineering, Xuzhou University of Technology, Xuzhou 221018, China*

Complete contact information is available at: https://pubs.acs.org/10.1021/acsomega.2c06782

## Notes

The authors declare no competing financial interest.

## REFERENCES

(1) Okabe, T.; Fukuda, K.; Takasaki, A.; Kakishita, K.; Yamamoto, R. Development of Renewable Woodceramics Synthesized from Cashew Nuts Shell Oil. *Open Journal of Composite Materials* **2021**, *11*, 23−30.
(2) Choi, N. S.; Chen, Z.; Freunberger, S. A.; Ji, X.; Sun, Y. K.; Amine, K.; Yushin, G.; Nazar, L. F.; Cho, J.; Bruce, P. G. Challenges Facing Lithium Batteries and Electrical Double-Layer Capacitors. *Angew. Chem., Int. Ed.* **2012**, *51*, 9994−10024.
(3) Taer, E.; Melisa, M. A.; Agustino, A.; Taslim, W. S.; Sinta Mustika, R.; Apriwandi, A. A green and low-cost of mesoporous electrode based activated carbon monolith derived from fallen teak leaves for high electrochemical performance. *Istrazivanja i Projektovanja za Privredu* **2021**, *19*, 1−12.
(4) He, H.; Shi, L.; Fang, Y.; Li, X.; Song, Q.; Zhi, L. Mass Production of Multi-Channeled Porous Carbon Nanofibers and Their Application as Binder-Free Electrodes for High-Performance Supercapacitors. *Small* **2014**, *10*, 4671−4676.
(5) Carbonized chicken eggshell membranes with 3D architectures as high-performance electrode materials for supercapacitors. *Adv. Energy Mater.***2012**, *2* (), 431-437.
(6) Abbas, Y.; Yun, S.; Wang, Z.; Zhang, Y.; Zhang, X.; Wang, K. Recent advances in bio-based carbon materials for anaerobic digestion: A review. *Renewable and Sustainable Energy Reviews* **2021**, *135*, 110378.
(7) (a) Li, Y.; Yang, W.; Han, L.; Li, H.; Wen, Z.; Li, Y.; Wang, X.; Sun, H.; Lu, T.; Xu, M.; Pan, L. Recent progress and perspective of multifunctional integrated zinc-ion supercapacitors. *Energy Materials* **2022**, *2*, 200018. (b) He, C.; Cheng, J.; Liu, Y.; Zhang, X.; Wang, B. Thin-walled hollow fibers for flexible high energy density fiber-shaped supercapacitors. *Energy Materials* **2021**, *1*, 100010.
(8) Liu, H.; Geng, C.; Wei, P.; Chen, H.; Zheng, S.; Wang, H.; Xie, Y. Improving the performance and stability of large-area carbon-based perovskite solar cells using N, O co-doped biomass porous carbon. *J. Alloys Compd.* **2022**, *912*, 165123.
(9) Petersen, E. J.; Huang, H. W. J. W.; Weber, W. J. Ecological Uptake and Depuration of Carbon Nanotubes by Lumbriculus variegatus. *Environ. Health Perspect.* **2008**, *116*, 496−500.
(10) (a) Gelardi, D. L.; Li, C.; Parikh, S. J. An emerging environmental concern: Biochar-induced dust emissions and their potentially toxic properties. *Sci. of The Total Environment* **2019**, *678*, 813−820. (b) Tang, Z.; Pei, Z.; Wang, Z.; Li, H.; Zeng, J.; Ruan, Z.; Huang, Y.; Zhu, M.; Xue, Q.; Zhi, C. Highly anisotropic, multichannel wood carbon with optimized heteroatom doping for supercapacitor and oxygen reduction reaction. *Carbon: An International Journal Sponsored by the American Carbon Society* **2018**, *130*, 532−543.
(11) (a) Sundriyal, S.; Shrivastav, V.; Sharma, M.; Mishra, S.; Deep, A. Significantly enhanced performance of rGO/TiO2 nanosheet composite electrodes based 1.8 V symmetrical supercapacitor with use of redox additive electrolyte. *J. Alloys Compd.* **2019**, *790*, 377−387. (b) Xu, M.; Yu, Q.; Liu, Z.; Lv, J.; Lian, S.; Hu, B.; Mai, L.; Zhou, L. Tailoring porous carbon spheres for supercapacitors. *Nanoscale* **2018**, *10*, 21604−21616.
(12) Mansuer, M.; Miao, L.; Zhu, D.; Duan, H.; Lv, Y.; Li, L.; Liu, M.; Gan, L. Facile construction of highly redox active carbons with regular micropores and rod-like morphology towards high-energy supercapacitors. *Materials Chemistry Frontiers* **2021**, *5*, 3061−3072.
(13) Dubey, P.; Shrivastav, V.; Maheshwari, P. H.; Sundriyal, S. Recent advances in biomass derived activated carbon electrodes for hybrid electrochemical capacitor applications: Challenges and opportunities. *Carbon* **2020**, *170*, 1−29.
(14) (a) Sesin, V.; Davy, C. M.; Freeland, J. R. Review of Typha spp. (cattails) as toxicity test species for the risk assessment of environmental contaminants on emergent macrophytes. *Environ. Pollut.* **2021**, *284*, 117105. (b) Hamad, M. T. M. H. Comparative study on the performance of Typha latifolia and Cyperus Papyrus on the removal of heavy metals and enteric bacteria from wastewater by surface constructed wetlands. *Chemosphere* **2020**, *260*, 127551.
(15) (a) Zhao, L.; Fan, L.-Z.; Zhou, M.-Q.; Guan, H.; Qiao, S.; Antonietti, M.; Titirici, M.-M. Nitrogen-Containing Hydrothermal Carbons with Superior Performance in Supercapacitors. *Adv. Mater.* **2010**, *22*, 5202−5206. (b) Wang, J.; Kaskel, S. KOH activation of carbon-based materials for energy storage. *J. Mater. Chem.* **2012**, *22*, 23710−23725.
(16) (a) Poli, F.; Momodu, D.; Spina, G. E.; Terella, A.; Mutuma, B. K.; Focarete, M. L.; Manyala, N.; Soavi, F. Pullulan-ionic liquid-based supercapacitor: A novel, smart combination of components for an easy-to-dispose device. *Electrochim. Acta* **2020**, *338*, 135872. (b) Momodu, D.; Sylla, N. F.; Mutuma, B.; Bello, A.; Masikhwa, T.; Lindberg, S.; Matic, A.; Manyala, N. Stable ionic-liquid-based symmetric supercapacitors from Capsicum seed-porous carbons. *J. Electroanal. Chem.* **2019**, *838*, 119−128. (c) Sylla, N. F.; Ndiaye, N. M.; Ngom, B. D.; Momodu, D.; Madito, M. J.; Mutuma, B. K.; Manyala, N. Effect of porosity enhancing agents on the electrochemical performance of high-energy ultracapacitor electrodes derived from peanut shell waste. *Sci. Rep.* **2019**, *9*, 13673.
(17) (a) Wang, X.; Yun, S.; Fang, W.; Zhang, C.; Liang, X.; Lei, Z.; Liu, Z. Layer-Stacking Activated Carbon Derived from Sunflower Stalk as Electrode Materials for High-Performance Supercapacitors. *ACS Sustainable Chem. Eng.* **2018**, *6*, 11397−11407. (b) Yang, C.; Yun, S.; Shi, J.; Sun, M.; Zafar, N.; Arshad, A.; Zhang, Y.; Zhang, L. Tailoring the supercapacitive behaviors of Co/Zn-ZIF derived nanoporous carbon via incorporating transition metal species: A hybrid experimental-computational exploration. *Chem. Eng. J.* **2021**, *419*, 129636. (c) Wang, Z.; Yun, S.; Wang, X.; Wang, C.; Si, Y.; Zhang, Y.; Xu, H. Aloe peel-derived honeycomb-like bio-based carbon with controllable morphology and its superior electrochemical properties for new energy devices. *Ceram. Int.* **2019**, *45*, 4208−4218.
(18) Deng, J.; Xiong, T.; Xu, F.; Li, M.; Han, C.; Gong, Y.; Wang, H.; Wang, Y. Inspired by bread leavening: one-pot synthesis of hierarchically porous carbon for supercapacitors. *Green Chem.* **2015**, *17*, 4053−4060.
(19) Kim, H.-J.; Ahn, Y.-S. Coating of chromium and titanium carbide on diamond particles in molten LiCl−KCl−NaCl. *J. Alloys Compd.* **2020**, *849*, 156508.
(20) (a) Kim, H.-J.; Choi, H.-L.; Ahn, Y.-S. Chromium carbide coating of diamond particles using low temperature molten salt mixture. *J. Alloys Compd.* **2019**, *805*, 648−653. (b) Kang, Q.; He, X.; Ren, S.; Zhang, L.; Wu, M.; Guo, C.; Cui, W.; Qu, X. Preparation of copper−diamond composites with chromium carbide coatings on diamond particles for heat sink applications. *Applied Thermal Engineering* **2013**, *60*, 423−429.
(21) (a) Bergna, D.; Hu, T.; Prokkola, H.; Romar, H.; Lassi, U. Effect of Some Process Parameters on the Main Properties of Activated Carbon Produced from Peat in a Lab-Scale Process. *Waste and Biomass Valorization* **2020**, *11*, 2837−2848. (b) Xia, C.; Shi, S. Q. Self-activation for activated carbon from biomass: theory and parameters. *Green Chem.* **2016**, *18*, 2063−2071.

(22) Mutuma, B. K.; Sylla, N. F.; Bubu, A.; Ndiaye, N. M.; Santoro, C.; Brilloni, A.; Poli, F.; Manyala, N.; Soavi, F. Valorization of biodigestor plant waste in electrodes for supercapacitors and microbial fuel cells. *Electrochim. Acta* **2021**, *391*, 138960.
(23) Li, Z.; Zhang, L.; Amirkhiz, B. S.; Tan, X.; Xu, Z.; Wang, H.; Olsen, B. C.; Holt, C. M. B.; Mitlin, D. Carbonized Chicken Eggshell Membranes with 3D Architectures as High-Performance Electrode Materials for Supercapacitors (Adv. Energy Mater. 4/2012). *Adv. Energy Mater.* **2012**, *2*, 430.
(24) Sundriyal, S.; Shrivastav, V.; Kaur, A.; Deep, S. R.; Dhakate, S. R. Surface and diffusion charge contribution study of neem leaves derived porous carbon electrode for supercapacitor applications using acidic, basic, and neutral electrolytes. *The Journal of Energy Storage* **2021**, *41*, 103000.
(25) Dutta, S.; Bhaumik, A.; Wu, K. C. W. Hierarchically porous carbon derived from polymers and biomass: effect of interconnected pores on energy applications. *Energy Environ. Sci.* **2014**, *7*, 3574−3592.
(26) Hao, L.; Ning, J.; Luo, B.; Wang, B.; Zhang, Y.; Tang, Z.; Yang, J.; Thomas, A.; Zhi, L. Structural Evolution of 2D Microporous Covalent Triazine-Based Framework toward the Study of High-Performance Supercapacitors. *J. Am. Chem. Soc.* **2015**, *137*, 219−225.
(27) Biswal, M.; Banerjee, A.; Deo, M.; Ogale, S. From dead leaves to high energy density supercapacitors. *Energy Environ. Sci.* **2013**, *6*, 1249−1259.
(28) Wang, Q.; Liu, F.; Jin, Z.; Qiao, X.; Huang, H.; Chu, X.; Xiong, D.; Zhang, H.; Liu, Y.; Yang, W. Hierarchically Divacancy Defect Building Dual-Activated Porous Carbon Fibers for High-Performance Energy-Storage Devices. *Adv. Funct. Mater.* **2020**, *30*, 2002580.
(29) Wang, D.-W.; Li, F.; Liu, M.; Lu, G. Q.; Cheng, H.-M. 3D Aperiodic Hierarchical Porous Graphitic Carbon Material for High-Rate Electrochemical Capacitive Energy Storage. *Angew. Chem., Int. Ed.* **2009**, *48*, 1525.
(30) Sun, C.; Guo, Z.; Zhou, M.; Li, X.; Cai, Z.; Ge, F. Heteroatoms-doped porous carbon electrodes with three-dimensional self-supporting structure derived from cotton fabric for high-performance wearable supercapacitors. *J. Power Sources* **2021**, *482*, 228934.



https://doi.org/10.1021/acsomega.2c06782
*ACS Omega* 2023, 8, 1353−1361